Paleoceanography and Paleoclimatology

Supporting Information for

Early to Middle Miocene Orbitally-Paced Climate Dynamics in the Eastern Equatorial Atlantic

Bianca R. Spiering[1], Evi Wubben[1], Frederik J. Hilgen[1], and Appy Sluijs[1]

[1]Department of Earth Sciences, Faculty of Geosciences, Utrecht University, Utrecht, The Netherlands

Contents of this file

Introduction

This Supporting Information contains additional figures that support the main text.

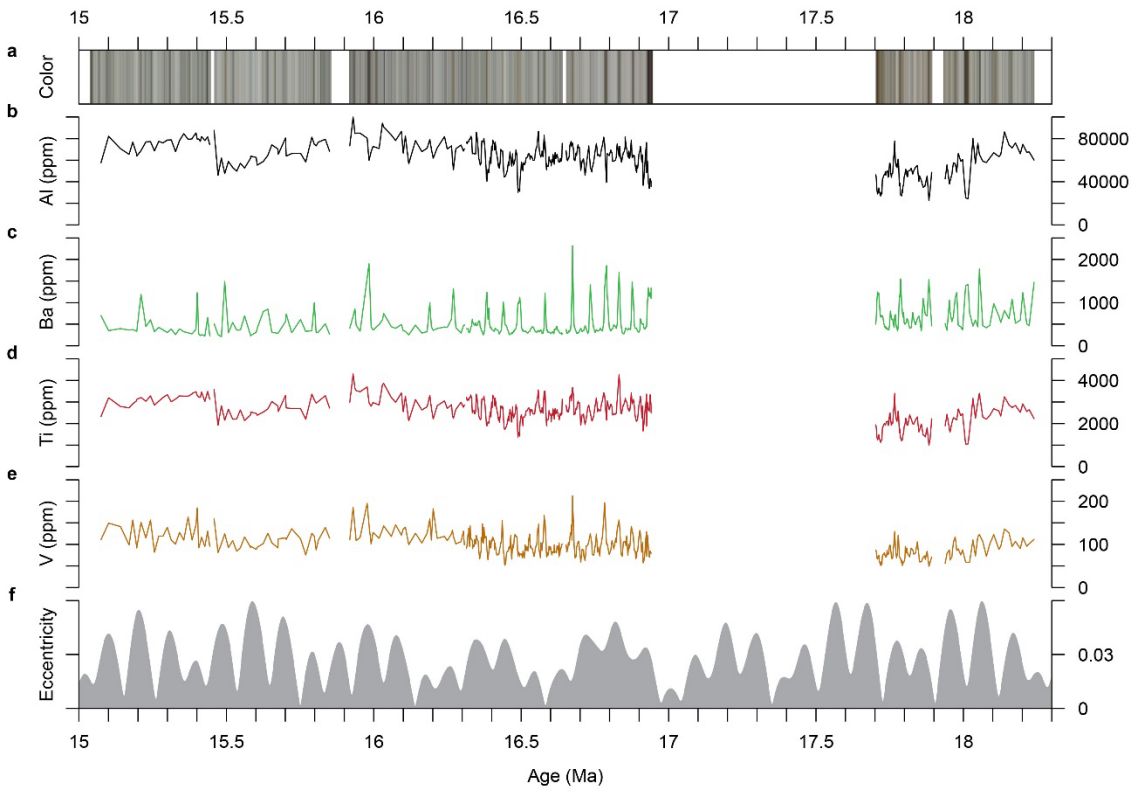

Figure S1. Overview of Early to Middle Miocene elemental concentrations from Site 959: (**a**) color, (**b**) Al, (**c**) Ba, (**d**) Ti, (**e**) V, and (**f**) the La2004 eccentricity solution (Laskar et al., 2004).

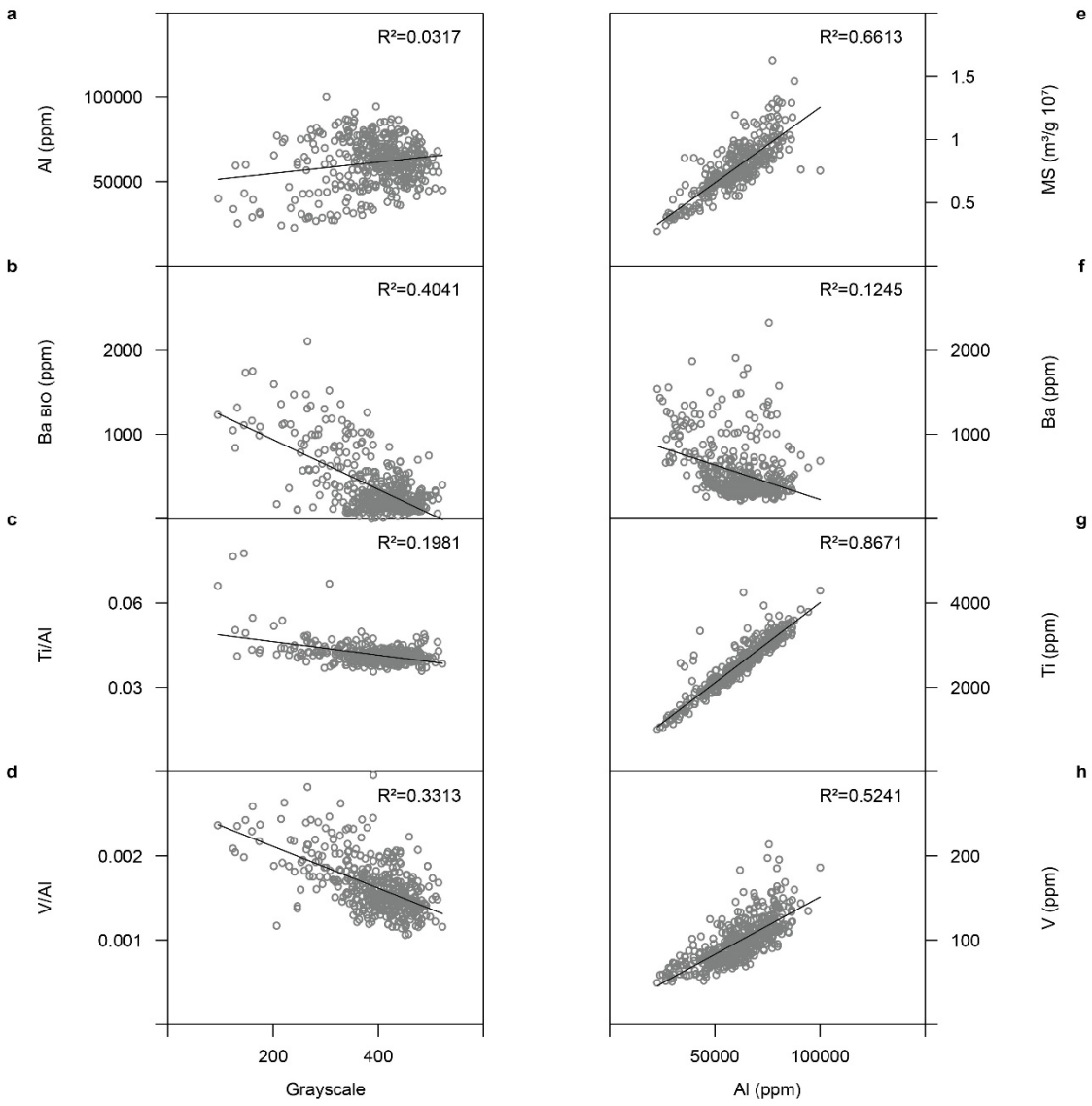

Figure S2. Scatter plots showing the relationship between Site 959 data. Grayscale is plotted against Al (**a**), Ba_{bio} (**b**), Ti/Al (**c**), and V/Al (**d**). Al is plotted against MS (**e**), Ba (**f**), Ti (**g**), and V (**h**). Linear trendlines (solid black) and R-squared values are indicated.

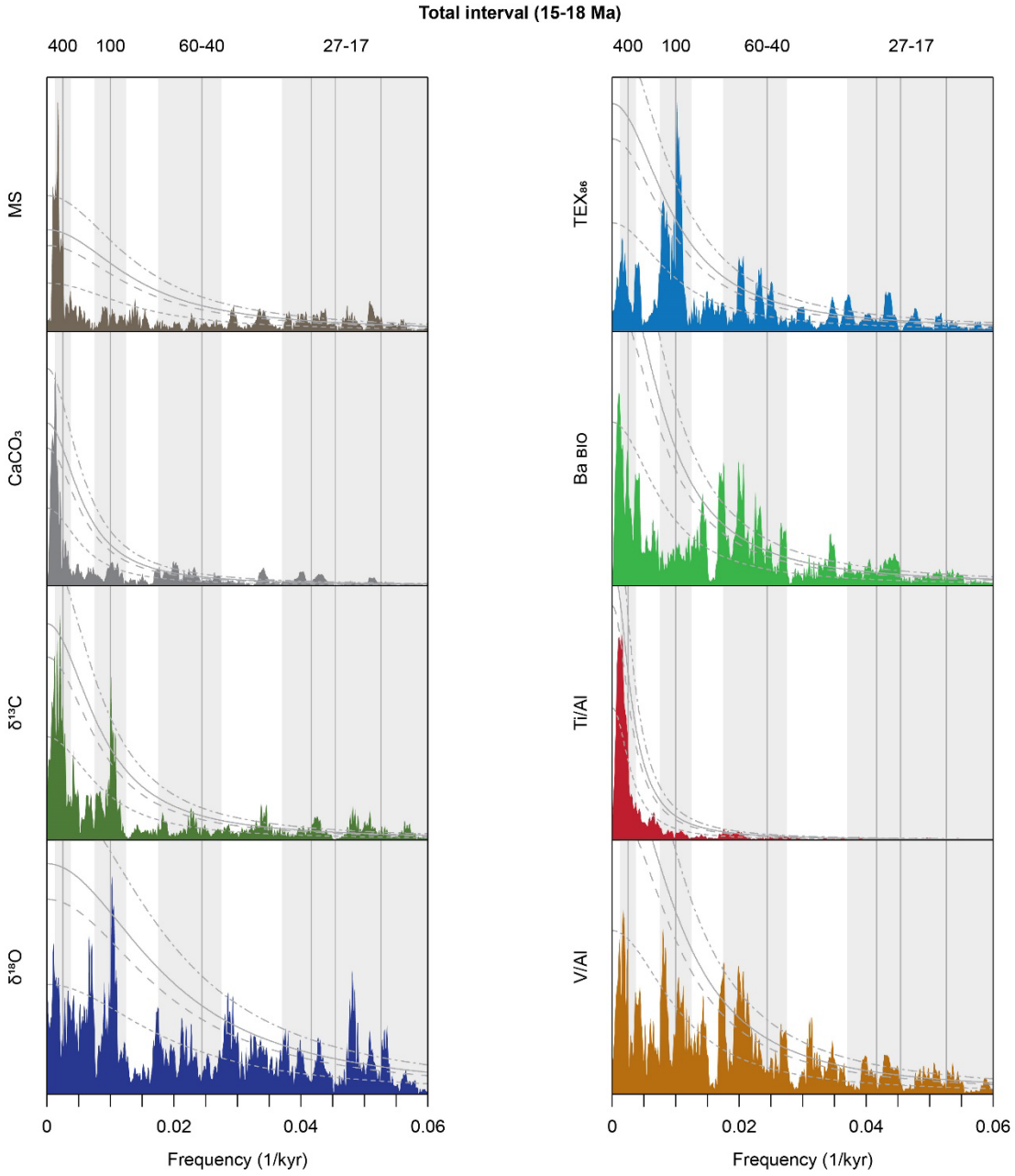

Figure S3. Power spectra of Site 959 proxy data for the total Early to Middle Miocene interval (18-15 Ma). A linear scale in used for both axes. AR1 fit, and 90%, 95%, and 99% confidence levels are indicated by the small dashed, large dashed, solid, small-large dashed gray lines, respectively. The gray bars indicate important frequency bands

representing periodicities of ~400 kyr, ~100 kyr, ~60-40 kyr, and ~27-17 kyr. The vertical gray lines indicate exact frequencies of 1/400, 1/100, 1/41, 1/24, 1/22, 1/19 1/kyr.

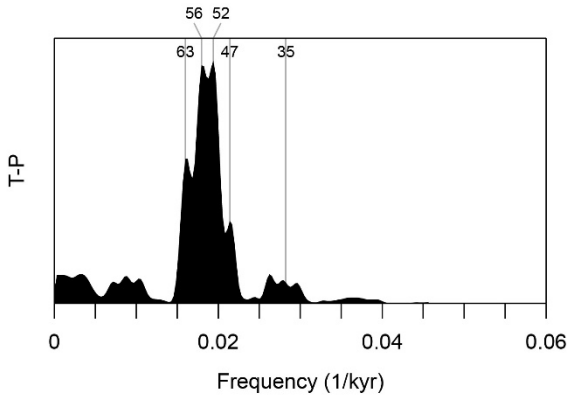

Figure S4. Power spectrum of the amplitude modulation of the standardized tilt and reversed-precession (T-P) curve for the interval 16.9-16.3 Ma. The vertical gray lines indicate periodicities (in kyr) of major peaks in the spectrum. Orbital solution is derived from La2004 (Laskar et al., 2004).

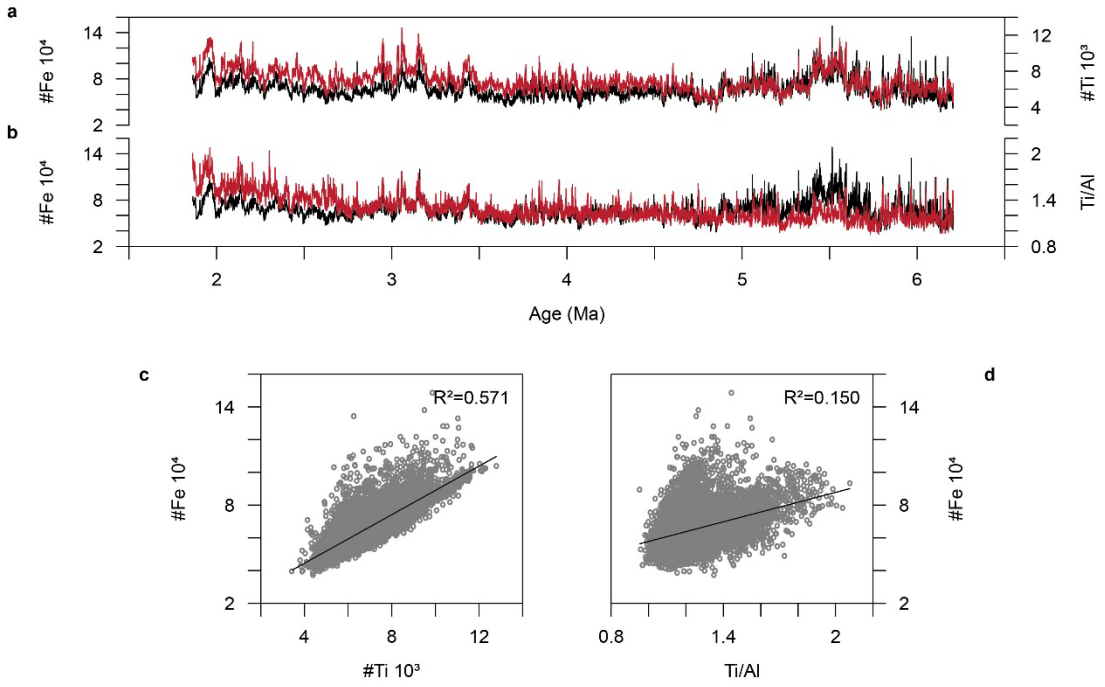

Figure S5. Fe intensity data compared to Ti intensity and Ti/Al data of Site 959 for the interval 2-6 Ma (Vallé et al., 2017). The Fe count record (black) is compared to Ti count (red; **a**) and Ti/Al (red; **b**). Scatter plots show the relationship between Fe count and Ti

count (**c**), and Fe count and Ti/Al (**d**). Linear trendlines (solid black) and R-squared values are indicated.

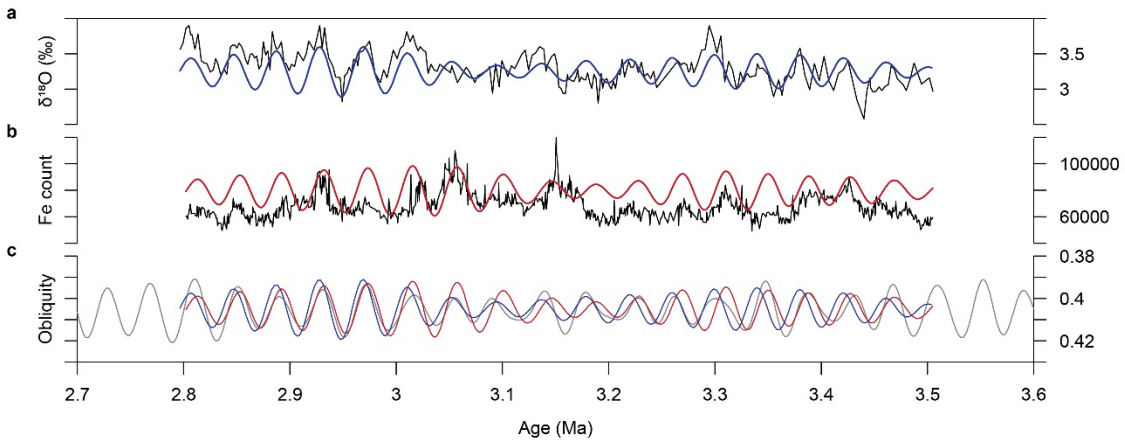

Figure S6. Benthic $\delta^{18}O$ (black; **a**) and Fe intensity data (black; **b**) of Site 959 for the 3.5-2.8 Ma interval. The data are derived from van der Weijst et al. (2020) and Vallé et al. (2017), respectively. Bandpass filters of ~41 kyr cyclicity in $\delta^{18}O$ (blue) and Fe (red) are compared to obliquity (gray; **c**) of the La2004 solution (Laskar et al., 2004). Data is

plotted on the revised age model of van der Weijst et al. (2020). The following bandpass filter widths (in 1/kyr) were used: 0.021-0.028 for $\delta^{18}O$, and 0.021-0.028 for Fe.

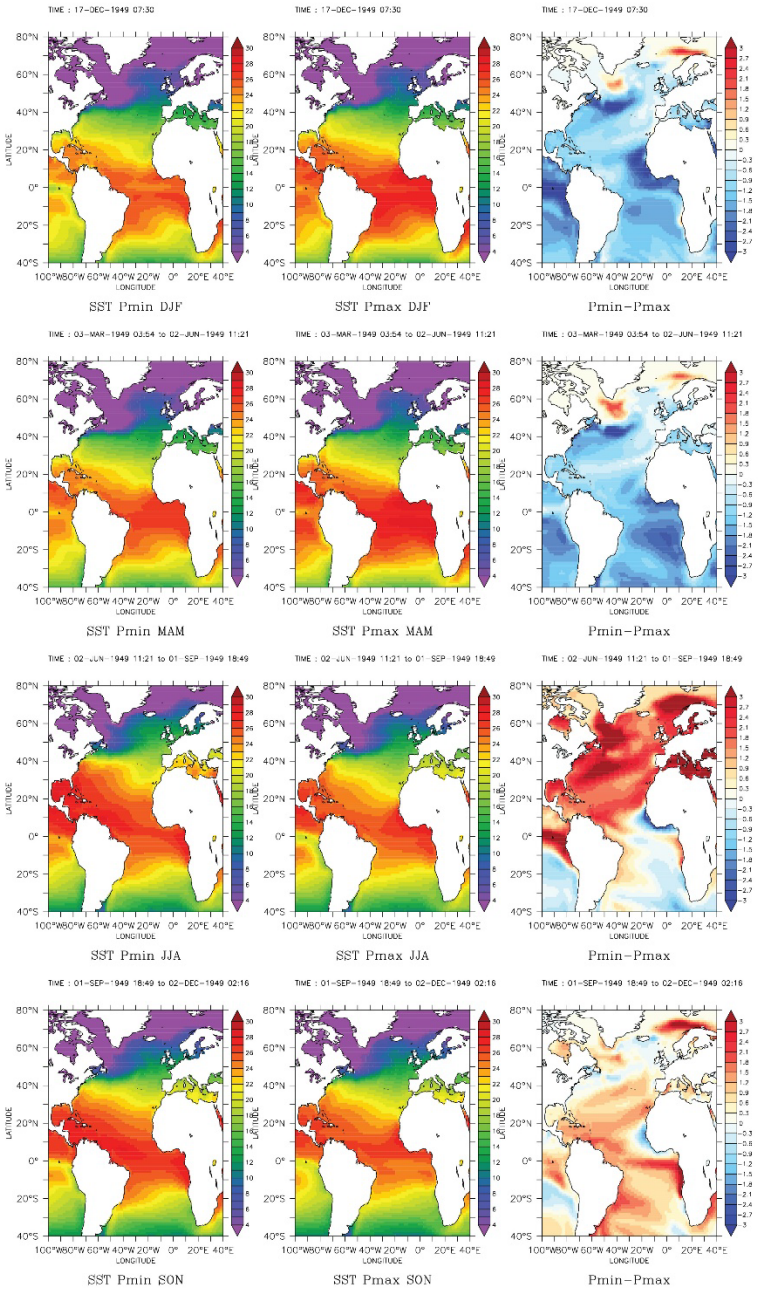

Figure S7. Sea surface temperature output of the model experiments of Bosmans, Drijfhout, et al. (2015). A high-resolution, coupled ocean-atmosphere, general circulation model was used. Experiments were performed with different orbital parameters: minimum precession and minimum obliquity (Pmin), and maximum precession and

minimum obliquity (Pmax). Outputs are shown for December to February (DJF), March to May (MAM), June to August (JJA), and September to November (SON).

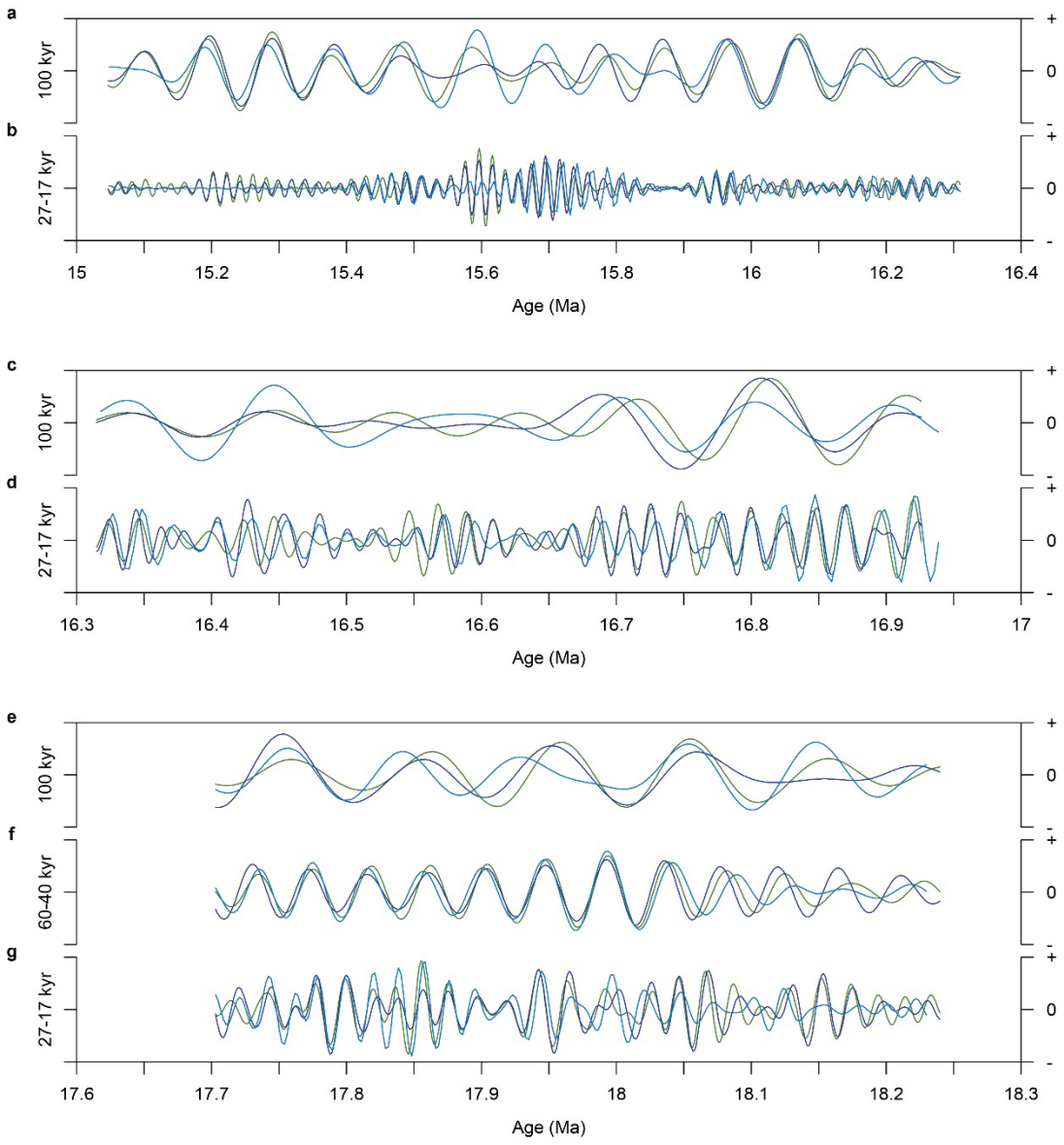

Figure S8. Phase relations between $\delta^{13}C$ (green), $\delta^{18}O$ (blue), and TEX_{86} (dark blue) on ~100 kyr, ~60-40 kyr, and ~27-17 kyr scales for three different intervals: 15.0-16.3 Ma (**a**), 16.3-16.9 Ma (**b**), and 17.7-18.2 Ma (**c**). See captions of Figures 6, 7, and 8 for bandpass filter widths.